Investigation of the conductivity of molten alkali and silver salts in the region between radio frequencies and the far-infrared

1989 J. Phys.: Condens. Matter 1 5253

(http://iopscience.iop.org/0953-8984/1/31/024)

J. Phys.: Condens. Matter 1 (1989) 5253–5262. Printed in the UK

Investigation of the conductivity of molten alkali and silver salts in the region between radio frequencies and the far-infrared

A Kasemann, H Happ and U Wienpahl
II. Physikalisches Institut der Universität zu Köln, Zülpicher Straße 77, D-5000 Köln, Federal Republic of Germany

Received 15 September 1988, in final form 4 January 1989

Abstract. The dynamical conductivity $\sigma(\omega)$ of molten $NaNO_2$ and $LiNO_3$ is measured near their melting points at frequencies between 0.5 MHz and 345 GHz (11.5 cm^{-1}) joining the far-infrared. Dispersion is found only in the microwave range from which a relaxation time of about 5×10^{-12} s is estimated for jump diffusion and is assumed to give the essential contribution to σ. From reflection measurements the far-infrared conductivity of all alkali nitrates in the liquid state is evaluated. It can be satisfactorily described by an expression derived from an oscillator equation formulated with a memory function composed of two exponentials. The short-time behaviour is characterised by a frequency parameter which scales with the reduced mass of the ions, suggesting that nearly equal effective forces are operative. Additional measurements between 0.5 and 110 MHz on various other molten alkali and silver salts also show no dispersion of the conductivity in this range.

1. Introduction

In a previous paper (Happ *et al* 1987) we presented the results of a far-infrared (FIR) and Raman investigation of molten $NaNO_2$ and $LiNO_3$. In particular, we evaluated the FIR conductivity $\sigma(\omega)$ and showed that this spectrum can be described quite well by the real part of a dynamical conductivity derived from a generalised oscillator equation formulated with a memory function composed of two exponentials. To obtain a complete picture of the conductivity in the transition from the high-frequency oscillatory to the low-frequency diffusive region, we have extended our measurements to the radio-frequency, microwave (MW) and millimetre wave range (from 0.5 MHz to 345 GHz). The present paper gives a detailed account of the results and the methods used in the different ranges. Preliminary MW results have already been indicated in our previous paper. They show that the conductivity does not drop monotonically to its DC value but passes through a minimum in this range. To find out whether the structure of the FIR conductivity of $LiNO_3$ and the possibility that it can be described by the expression derived from the memory function equation mentioned above is a common feature of the alkali nitrates, we have measured and analysed the FIR reflection spectra of these molten salts. Special attention was paid to the experimentally difficult region near 10 cm^{-1} to estimate the behaviour of σ approaching the millimetre wave region.

In molten $NaNO_2$ and $LiNO_3$, no further dispersion of σ was observed below the MW range. On the contrary, Taniguchi *et al* (1983) in a paper on the AC conductivity of

0953-8984/89/315253 + 10 $02.50

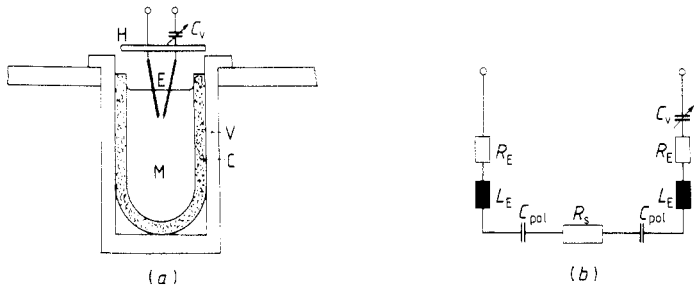

Figure 1. (*a*) Experimental arrangement for the megahertz measurements: E, platinum electrodes of diameter 0.5 mm, tightly fitting in ceramic tubules, free tips of length 2 mm and 4 mm apart; C, ceramic crucible; V, stainless steel container; H, heat shield; M, melt. (*b*) The equivalent circuit shows the circuit elements representing the electrodes, the sample, possible polarisation capacities at the electrodes and a variable capacitor for compensating purposes.

molten sodium salts reported dispersion already in the megahertz region. Stimulated by this report, we incorporated in our measurements between 0.5 and 110 MHz some selected alkali and silver salts (NaCl, NaBr, AgCl, AgBr, $NaNO_3$ and KNO_3). In these melts, too, no dispersion was found in the frequency range considered.

2. Experimental details

The FIR reflection spectra of the molten anhydrous alkali nitrates have been measured near their melting points from 10 to 600 cm^{-1} with a FIR Fourier spectrometer in the arrangement described by Happ *et al* (1987). The sample chamber was filled with dry N_2 under atmospheric pressure. A Kramers–Kronig analysis was applied to evaluate the dielectric function $\hat{\varepsilon}(\omega)$ and to calculate the FIR conductivity $\sigma = \varepsilon_0 \omega \, \mathrm{Im}[\hat{\varepsilon}(\omega)]$ (ε_0 denotes the permittivity of free space). In this analysis the reflection spectra were completed by data measured in the near-infrared and by a suitable extrapolation to $R = 1$ below 10 cm^{-1}. For $LiNO_3$ the low-frequency data could be used. In the following, we describe the different methods applied to determine the conductivity of molten $NaNO_2$ and $LiNO_3$ in the region between 0.5 MHz and 345 GHz (11.5 cm^{-1}). In the megahertz range, additional measurements have been performed on the selected salts indicated in § 1.

In the region from 0.5 to 110 MHz the conductivity was derived from the resistance of the melt between the tips of two platinum electrodes. Figure 1(*a*) shows the experimental arrangement. The molten salts were kept in a ceramic crucible and heated through a stainless steel container by a gas burner with an uncertainty in temperature of ±10 K. Electrical heating was avoided because it led to serious difficulties due to unwanted high-frequency stray currents induced in the measuring circuit. In figure 1(*b*) is the equivalent circuit of the electrode system including a variable capacitor C_v. (The very small capacity between the electrodes could be neglected.) The modulus $|\hat{Z}|$ and the phase φ of its impedance was measured with a vector meter (HP-4815A), and the sample resistance R_s was calculated from $R_s + 2R_E = |\hat{Z}| \cos\varphi$. The electrode resistance $2R_E$ varied between 32 and 225 mΩ owing to the skin effect and was determined at each frequency by a short-circuit measurement. With increasing frequency the impedance of the sample circuit became dominated by the inductive reactance of the electrodes, and φ became close to 90°. To obtain the real part with sufficient accuracy the variable capacitor C_v

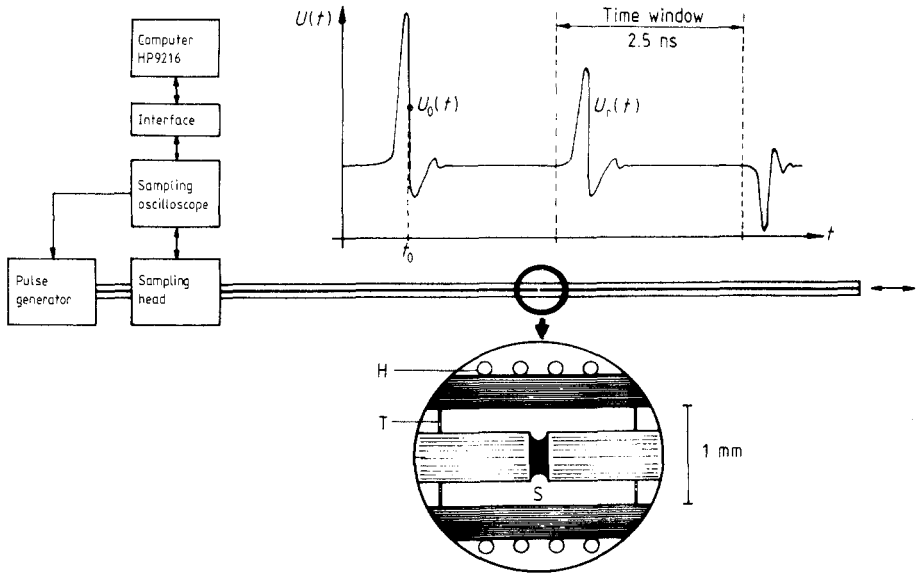

Figure 2. Schematic diagram of the experimental arrangement for time domain spectroscopy: $U_0(t)$, primary pulse; $U_r(t)$, reflected pulse; t_0, time reference at half-height between the maximum and the following minimum of the pulse; H, heater; T, thin Teflon spacers; S, sample.

served largely to compensate this inductive contribution. R_s is related to the conductivity by $R_s = K/\sigma$ where K is the cell constant describing the current distribution between the electrodes. K was determined using a 3M KCl solution at room temperature with $\sigma(\text{KCl}) = 0.2981\ \Omega^{-1}\,\text{cm}^{-1}$ (table of Landolt–Börnstein). The resistance of the KCl solution between the electrodes was constant and equal to $14.0 \pm 0.5\ \Omega$ from 0.5 to 110 MHz.

In the range between 0.3 and 8 GHz, time domain spectroscopy with short voltage pulses was applied as described by Voss and Happ (1984). The schematic diagram of the experimental set-up with the special sample arrangement in a coaxial transmission line is shown in figure 2. In this method the properties of a sample are derived from its reflection response function $\hat{r}(\omega)$. This function is obtained as the ratio of the Fourier transform of the voltage pulse reflected at the sample to that of the reference pulse reflected at the end of the empty open transmission line.

Terminating the transmission line with a cell filled with the conductive salt results in a reflection coefficient $|\hat{r}|$ of about unity or less in the frequency range considered, and σ cannot be determined with sufficient accuracy. Therefore we placed the sample as a liquid bridge in a gap between the inner conductors of the line, as shown in figure 2. The width of the gap could be adjusted to give the bridge a suitable resistance but was always smaller than the wavelengths contained in the voltage pulses. Thus the sample can be represented by a series impedance Z_s in the line. With the typical dimensions $r_0 \simeq 0.1$ mm (waist radius), $r_a = 0.25$ mm (radius of the inner conductor) and $L \simeq 0.3$ mm (gap width), Z_s was about 40 Ω for the salts measured, leading to a reflection coefficient of between 0.3 and 0.4. To realise the open transmission line needed for the reference measurement the second part of the inner conductor could be withdrawn. The outer conductor was given a square cross section for technical reasons. The heatable section of the line containing the sample was made of stainless steel and could be opened to insert the sample and to measure its dimensions.

The transmission line behind the sample was given such a length that the signal reflected from the end termination was outside the time window needed to measure the pulse reflected at the sample. Thus the transmission line can be considered as terminated by the series impedance $Z = Z_s + Z_0$, where $Z_0 = 50\ \Omega$ is the line impedance, and we obtain for $\hat{r} = (Z - Z_0)/(Z + Z_0)$

$$\hat{r} = Z_s/(2Z_0 + Z_s). \tag{1}$$

As the skin depth of the sample is larger than the bridge radius, Z_s was calculated by integration over the contributions of slice of radius $r(x)$. For $r(x)$ we choose the function $r(x) = r_0 \cosh(2ax/L)$ where the parameter a is determined from $r(L/2) = r_a$. This profile $r(x)$ is correct if the pressure difference between the interior and the exterior of the bridge surface is zero. Detailed information on bridge profiles calculated for various physical and geometrical conditions is reproduced in an article by Martinez *et al* (1984). Making use of this information, we find that for the typical dimensions of our samples the profile chosen is a good approximation and gives the relation

$$Z_s = (L/a\pi r_0^2\sigma) \tanh a. \tag{2}$$

Within the accuracy of measurement, $\pm 0.05\ \Omega^{-1}\ \mathrm{cm}^{-1}$, Z_s and, hence, σ turned out to be real.

In the range between 10 and 100 GHz, waveguide techniques were applied using hybrid tees to measure the reflection coefficient of the molten salts in the X, Q and E bands. In each case a heatable stainless steel waveguide section connected to one arm of a tee and sealed by a thin mica window was filled with the melt. The melt was of sufficient length to avoid multiple reflections. Thus the reflection coefficient $\hat{r}$ is that of its plane surface and is given in a waveguide operated in the H_{10} mode by (Montgomery 1947)

$$\hat{r} = \{1 - [(\hat{\varepsilon} - p)/(1 - p)]^{1/2}\}/\{1 + [(\hat{\varepsilon} - p)/(1 - p)]^{1/2}\} \tag{3}$$

where $p = (\lambda_0/\lambda_c)^2$, and λ_0 and λ_c are the wavelength in free space and the cut-off wavelength, respectively.

The millimetre wave measurements above 100 GHz were performed with a dispersive Michelson interferometer using Gaussian beam mirror optics and wire grids as polarising beam splitters. This instrument was built in our laboratory by Briskot (1986) according to the principles published by Parker *et al* (1978), with some modifications of the optics including phase modulation of the optical path difference produced by the moving Michelson mirror. Several millimetre wave oscillators were available between 100 and 345 GHz. The fixed Michelson mirror could be precisely replaced by the surface of the melt which was in a stainless steel vessel sealed with a thin quartz window. From the sample and reference interferograms, taking into account the effect of the quartz window, the complex reflection coefficient $\hat{r} = (1 - \sqrt{\hat{\varepsilon}})/(1 + \sqrt{\hat{\varepsilon}})$ of the melt at nearly perpendicular incidence can be determined.

3. Results

3.1. Megahertz range

As mentioned in § 1, the conductivities of several selected alkali and silver salts have been measured including two sodium salts which were reported to exhibit dispersion in the megahertz range by Taniguchi *et al* (1983). In contrast, our data measured about

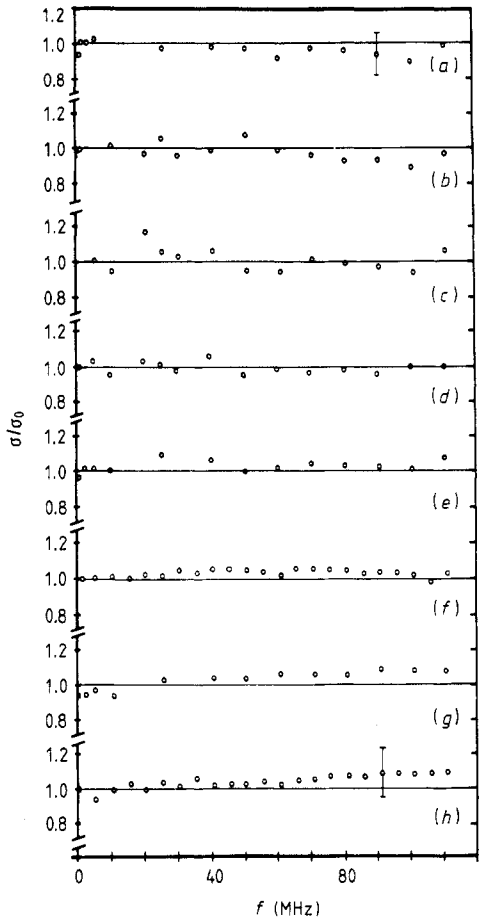

Figure 3. The conductivity of selected molten salts in the megahertz range near their melting points: (*a*) NaCl, $T = 1173$ K, $\sigma_0 = 3.58\ \Omega^{-1}\,cm^{-1}$; (*b*) NaBr, $T = 1043$ K, $\sigma_0 = 2.85\ \Omega^{-1}\,cm^{-1}$; (*c*) AgCl, $T = 873$ K, $\sigma_0 = 4.19\ \Omega^{-1}\,cm^{-1}$; (*d*) AgBr, $T = 773$ K, $\sigma_0 = 3.00\ \Omega^{-1}\,cm^{-1}$; (*e*) $NaNO_2$, $T = 573$ K, $\sigma_0 = 1.26\ \Omega^{-1}\,cm^{-1}$; (*f*) $LiNO_3$, $T = 553$ K, $\sigma_0 = 0.90\ \Omega^{-1}\,cm^{-1}$; (*g*) $NaNO_3$, $T = 593$ K, $\sigma_0 = 0.97\ \Omega^{-1}\,cm^{-1}$; (*h*) KNO_3, $T = 663$ K, $\sigma_0 = 0.66\ \Omega^{-1}\,cm^{-1}$. σ_0 is taken from a table of *Landolt–Börnstein*.

10 K above the respective melting points do not reveal, within the limits of accuracy, a frequency dependence of the conductivity up to 110 MHz, (figure 3). The DC conductivities, which vary between about 1 and 4 $\Omega^{-1}\,cm^{-1}$ near the melting points were taken from the Landolt–Börnstein tables. The discrepancy between our data on NaCl and NaBr and those of Taniguchi *et al* might be due to a shortcoming in their measurement. They placed the sample as a liquid bridge between two thin platinum electrodes and determined its resistance from a current measurement with the help of a small resistance connected in series. However, their calculation does not take proper account of the inductive reactance of the electrodes which becomes important at high frequencies as outlined in § 2.

For one of the salts, $LiNO_3$ (melting point, 526 K), we investigated the variation in σ with temperature between 533 and 793 K at 0.7 and 100 MHz. σ increases from 0.86 to 2.4 $\Omega^{-1}\,cm^{-1}$ but follows the same curve at both frequencies within experimental error. In figure 4 we present an Arrhenius plot of the molar conductance $\Lambda = \sigma V_m$. The variation in the molar volume $V_m = (0.015\ cm^3\ mol^{-1}\ K^{-1})$ was extracted from a paper by Pilz and Tödheide (1973). The molar conductance can be well described by $\Lambda = \Lambda_0 \exp(-U/k_B T)$ in the temperature region considered with $\Lambda_0 = 1050\ cm^2\ \Omega^{-1}\ mol^{-1}$ and the activation energy $U = 0.15$ eV or 15 kJ mol^{-1}. This is in reasonable agreement with the value given by Pilz and Tödheide (1973).

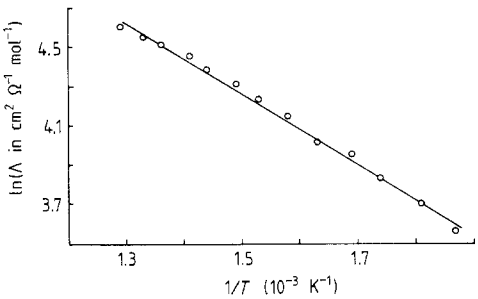

Figure 4. Arrhenius plot of the molar conductance of $LiNO_3$ at 0.7 MHz. The same data are valid at 100 MHz within experimental error.

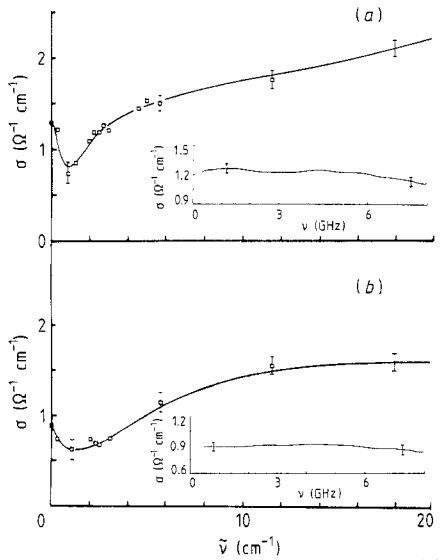

Figure 5. The MW and wave conductivity of (*a*) $NaNO_2$ at $T = 573$ K and (*b*) $LiNO_3$ at $T = 553$ K. The curves between 12 and 20 cm^{-1} represent FIR data.

3.2. MW and millimetre wave range

In this range the conductivities of $NaNO_2$ and $LiNO_3$ were determined continuously between 0.3 and 8 GHz and at discrete frequencies between 9.5 and 345 GHz (11.5 cm^{-1}). The results are shown in figure 5. The curves between 10 and 20 cm^{-1} represent FIR data which join the last millimetre wave point at 11.5 cm^{-1} within the measurement error. At the lower end of the range, σ is equal to the relevant DC conductivity σ_0. In both cases the conductivity remains nearly constant up to 8 GHz and passes through a minimum near 30 GHz. This behaviour is similar to that observed in the MW conductivity of AgJ-type superionic conductors in which the dispersion occurs at somewhat lower frequencies between 4 and 8 GHz (Funke 1976).

The dynamic conductivity in superionic conductors is usually discussed on the basis of a model in which the mobile ions oscillate at their lattice sites and move about by jump diffusion between equivalent sites. In a simple treatment of this model, Hubermann and Sen (1974) and Sen and Hubermann (1975) described the motion of the mobile ions by a Debye spectrum of damped oscillators and a Langevin equation below a cut-off frequency given by the hopping frequency of the jump processes. Neglecting correlations between the particles, they derived an expression for the conductivity which is a superposition of a Drude term and an oscillator term and can represent the general structure in the MW region.

A similar consideration may be applied to the molten salts. As for example Frenkel (1955) pointed out, gaps will exist in a liquid owing to thermal fluctuations, allowing jump diffusion of the particles. This model was used by Bockris *et al* (1960) to calculate the DC conductivity of various molten salts. In the interpretation of our MW and millimetre wave results, we also assume that jump diffusion gives an essential contribution to the low-frequency conductivity and that the total conductivity is a superposition of a Drude term and a term corresponding to the low-frequency wing of the oscillatory motion.

However, equation (4) with parameters appropriate to give a good fit to our FIR data is not suitable for constructing such a superposition. The resulting σ drops monotonically to values near σ_0 and, below 10 cm^{-1}, always remains above the MW data. As

Table 1. Parameters for equation (4) (c is the velocity of light).

	ω_1 (cm^{-1})	γ_1 (cm^{-1})	ω_2 (cm^{-1})	γ_2 (cm^{-1})	$S/2\pi c$ ($\Omega^{-1}\,cm^{-2}$)	T (K)
$LiNO_3$	176	17	326	329	2.99×10^3	553
$NaNO_3$	70	4.5	198	206	7.85×10^2	623
KNO_3	59	10.5	160	182	5.28×10^2	623
$RbNO_3$	57	10.8	123	186	3.20×10^2	623
$CsNO_3$	54	11.5	116	180	2.65×10^2	723

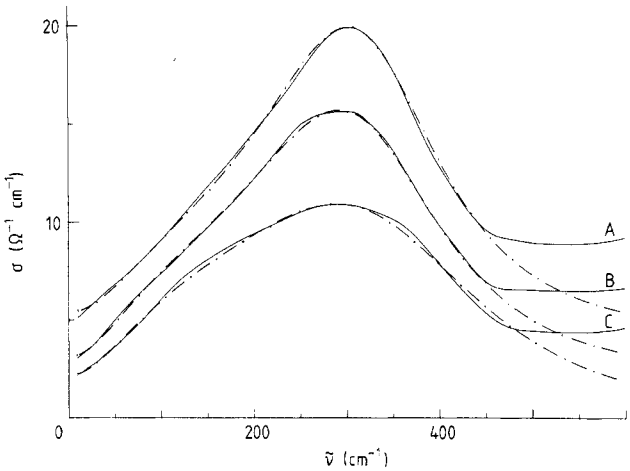

Figure 6. The FIR conductivity of $LiNO_3$ in the liquid state at $T = 553$ K ($\sigma_0 = 0.90\ \Omega^{-1}\,cm^{-1}$) (curves A), $T = 623$ K ($\sigma_0 = 1.33\ \Omega^{-1}\,cm^{-1}$) (curves B) and $T = 723$ K ($\sigma_0 = 1.84\ \Omega^{-1}\,cm^{-1}$) (curves C): —·—, calculated according to equation (4). The upper curves are shifted by a multiple of two units.

an estimate of the relaxation frequencies in the Drude term assumed, we take the positions of the conductivity minima which are at 26 GHz and 30 GHz for $NaNO_2$ and $LiNO_3$, respectively. From $2\pi\nu\tau = 1$ we obtain the nearly equal relaxation times $\tau = 5.3 \times 10^{-12}$ s. A second estimate is obtained from the usual expression for the jump probability per unit time: $w = \nu_0 \exp(-U/k_B T)$ where the activation energy given in § 3.1 is taken for U. The broad spectrum of the FIR response does not give an unambiguous value for the attempt frequency ν_0. As an upper limit, we take the frequency corresponding to ω_2 in table 1 which is related to short-time oscillations of the ions. For $LiNO_3$ at 553 K, we obtain $\tau = 2.4 \times 10^{-12}$ s, in agreement with the estimate from the MW data within a factor of 2.

3.3. *FIR conductivity of the alkali nitrates*

Figures 6 and 7 show the FIR conductivities derived from reflection measurements at $T/T_f = 1.05$, i.e. near the melting points The melting points T_f were taken from Ubbelohde (1978). In figure 7, which shows the conductivity of $LiNO_3$, the results at elevated temperatures are included. In all cases the FIR part of the structure can be quite well described by the real part of the expression (Happ *et al* 1987)

$$\hat{\sigma} = S/[-i\omega + \omega_1^2/(-i\omega + \gamma_1) + \omega_2^2/(-i\omega + \gamma_2)]. \tag{4}$$

It represents an oscillator with frequency-dependent eigenfrequency and damping. The

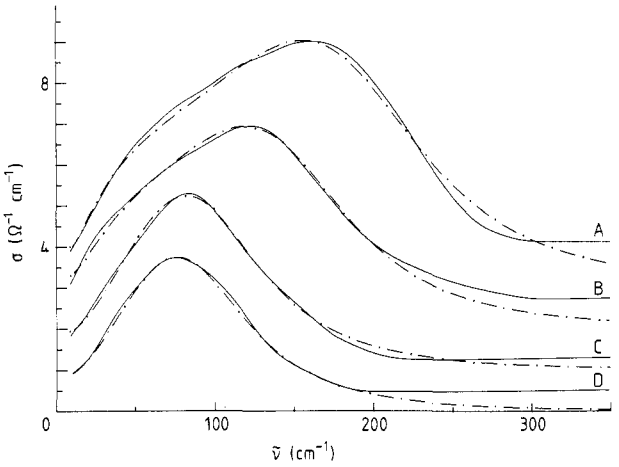

Figure 7. The FIR conductivity of $NaNO_3$ ($\sigma_0 = 1.15\ \Omega^{-1}\,cm^{-1}$) at $T = 623$ K (curves A), KNO_3 ($\sigma_0 = 0.66\ \Omega^{-1}\,cm^{-1}$) at $T = 623$ K (curves B), $RbNO_3$ ($\sigma_0 = 0.51\ \Omega^{-1}\,cm^{-1}$) at $T = 623$ K (curves C) and $CsNO_3$ ($\sigma_0 = 0.60\ \Omega^{-1}\,cm^{-1}$) at $T = 723$ K (curves D): —·—, calculated according to equation (4). The upper curves are shifted by a multiple of one unit.

parameters used at $T/T_f = 1.05$ to give a good fit to the FIR data are compiled in table 1. Near 10 cm^{-1} the theoretical curves start to deviate from the experimental curves and drop monotonically to values near σ_0. As already mentioned in § 3.2, this low-frequency behaviour does not allow a curve to be constructed which reproduces the conductivity minimum in the MW region observed for $LiNO_3$ (and $NaNO_2$). A fit of these low-frequency data up to 10 cm^{-1} is possible if one uses, independently of equation (4), a heavily damped oscillator superposed on a Drude term. The relaxation time of this term is 7 ps, in reasonable agreement with the earlier estimates. The experimental curve of $NaNO_3$ has already reached the value σ_0 at 10 cm^{-1} and has a steep slope. Therefore it can be expected that the conductivity of this system also passes through a minimum in the MW region. Within the limits of error, the tendency of the steep curve for KNO_3 still allows such a minimum, whereas the data for $RbNO_3$ and $CsNO_3$ tend monotonically to σ_0.

Equation (4) for $\hat{\sigma}$ is derived from a generalised oscillator equation containing two exponentials as a memory function. One of these, $\omega_2^2 \exp[-\gamma_2(t - t')]$, is related to the heavily damped short-time oscillation of the ionic components relative to each other and essentially determines the high-frequency wing of the conductivity. It decays with time constants $\tau_2 = 1/\gamma_2$ between 0.016 and 0.03 ps according to the data given in table 1 ($\gamma = 2\pi c$ (γ in cm^{-1})). Where data are available, ω_2 is found to be quite close to the frequency of the highest translational mode of the crystal. Using the frequencies given in table 1, we find that ω_2^2 scales with the inverse of the reduced mass of the salts: $\omega_2^2 M_r = 6.1 \times 10^5 \pm 10\%$ (ω^2 in units of reciprocal centimetres and M_r in atomic mass units). Thus the short-time oscillations can be viewed as the relative motion of orientationally randomised NO_3 groups and alkali ions under the action of nearly the same effective forces. The second part of the memory function with the smaller parameters

ω_1 and γ_1 is needed to reproduce the low-frequency wing of the conductivity. It indicates an oscillatory response of the liquid still at lower excitation frequencies where configurational compliance may be expected to reduce the effective forces. This term decays with a time constant τ_1 of about 0.5 ps.

If we write $\hat{\sigma}$ in the oscillator form (Happ *et al* 1987) the frequency-dependent eigenfrequency and damping are

$$\Omega^2(\omega) = \omega^2[\omega_1^2/(\omega^2 + \gamma_1^2) + \omega_2^2/(\omega^2 + \gamma_2^2)] \tag{5}$$

$$\gamma(\omega) = \omega_1^2\gamma_1/(\omega^2 + \gamma_1^2) + \omega_2^2\gamma_2/(\omega^2 + \gamma_2^2). \tag{6}$$

With the low values for γ_1 and the high values for γ_2 (see table 1), it turns out that the ω_2^2-term in Ω^2 decreases continuously with decreasing frequency throughout the whole FIR range considered, whereas the first term gives the nearly constant contribution ω_1^2 down to $\omega \simeq 3\gamma_1$, i.e. about 40 cm^{-1}, thus maintaining the oscillatory response. In the damping function $\gamma(\omega)$ the term characterised by γ_1 becomes important only below $\omega \simeq 3\gamma_1$ and gives the main contribution at lower frequencies. The term characterised by γ_2 decreases only slowly up to frequencies near ω_2 and determines the damping in the main part of the FIR.

As a further result, we find that in all nitrates the oscillator strength $S = ne^2/M_r$, determined as a fit parameter, has a value equal to that calculated with the number density n of ion pairs of the solid state within 10%. This is consistent with the picture that the increase in volume of the melt is mainly due to holes.

In the interpretation of our experimental data, three time constants τ, τ_1 and τ_2 are involved. These have been related to, for example, results of Raman studies of the collective modes in molten alkaline-earth halides by Bunten *et al* (1984, 1986) with due caution because of the different interpretations of infrared and Raman data. In these Raman spectra a time constant $\tau_{23} \simeq 1$ ps is associated with the broadening of the central peak and related to the electrical conductivity. It compares favourably with $\tau \simeq 2$–5 ps evaluated from our MW data. An average time constant τ_{45} associated with the width of the non-central structure has values of about 0.1 ps in the different melts. This lies between the values of the decay constants τ_1 and τ_2 of our memory functions. Thus it appears that, in the molten salts considered, a time constant of the order of 1 ps is associated with the electrical conductivity whereas time constants of the order of 0.1–0.01 ps are related to the damping of the collective modes.

4. Summary

The dynamical conductivities of molten $NaNO_2$ and $LiNO_3$ have been determined near their melting points at frequencies between 0.5 MHz and 345 GHz (11.5 cm^{-1}), joining the FIR region. In both cases the conductivity remains nearly constant up to the MW range where it passes through a minimum. Assuming that jump diffusion in the molten state gives an essential contribution in this region, we estimate a relaxation time for this process of about 5×10^{-12} s. From a systematic investigation of the FIR reflection spectra of the alkali nitrates in the liquid state, we derived their FIR conductivities near their melting points and at some elevated temperatures in the case of $LiNO_3$.

Although the structure of the conductivity of the various salts show some variation, it can be quite well described by a theoretical expression derived from a generalised oscillator equation including a simple memory function composed of two exponential terms. A frequency parameter relevant to the short-time behaviour scales with the

reduced mass of the salts, thus indicating a relative motion of the cations and the orientationally randomised NO_3 ions under nearly the same effective forces. The investigation is supplemented by conductivity measurements on some selected alkali and silver salts in the range between 0.5 and 110 MHz. In this range, no dispersion was observed in the salts considered, and the data coincided with the DC values within experimental error.

Acknowledgment

We wish to express our thanks to the Max-Planck Institut für Radioastronomie, Bonn, for making available to us a vector meter and millimetre wave oscillator.

References

Bockris J O'M, Crook E H, Bloom H and Richards N E 1960 *Proc. R. Soc.* A **225** 558
Briskot M 1986 *Diplomarbeit* Köln
Bunten R A J, McGreevy R L, Mitchell E W J and Raptis C 1986 *J. Phys. C: Solid State Phys.* **19** 2925
Bunten R A J, McGreevy R L, Mitchell E W J, Raptis C and Walker P J 1984 *J. Phys. C: Solid State Phys.* **17** 4705
Frenkel J 1955 *Kinetic Theory of Liquids* (New York: Dover)
Funke K 1976 *Prog. Solid State Chem.* **11** 345
Happ H, Böhm T, Kasemann A and Neuerbourg R 1987 *J. Phys. C: Solid State Phys.* **20** 5889
Hubermann B A and Sen P N 1974 *Phys. Rev. Lett.* **33** 1379
Landolt–Börnstein New Series 1960 vol II/7, 6. Auflage, ed. K–H Hellwge (Berlin: Springer)
Martinez I, Haynes J M and Langbein D 1987 *Fluid Sciences and Materials Science in Space* ed. H U Walter (Berlin: Springer)
Montgomery C 1947 *Technique of Microwave Measurements* (New York: McGraw-Hill)
Parker T J, Ledsham D A and Chambers W G 1978 *Infrared Phys.* **18** 179
Pilz V and Tödheide K 1973 *Ber. Bunsenges. Phys. Chem.* **77** 29
Sen P N and Hubermann B A 1975 *Phys. Rev. Lett.* **34** 1059
Taniguchi Y, Haruno M, Morinaga K and Yanagase T 1983 *J. Japan Inst. Met.* **47** 747
Ubbelohde A R 1978 *The Molten State of Matter* (New York: Wiley)
Voss G and Happ H 1984 *J. Phys. E: Sci. Instrum.* **17** 981